IOP Publishing Superconductor Science and Technology
Supercond. Sci. Technol. 31 (2018) 015003 (7pp) https://doi.org/10.1088/1361-6668/aa94ac

Transport properties of $Li_x(NH_3)_yFe_2(Te_zSe_{1-z})_2$ single crystals in the mixed state

Shanshan Sun, Shaohua Wang, Chenghe Li and Hechang Lei

Department of Physics and Beijing Key Laboratory of Opto-electronic Functional Materials & Micro-nano Devices, Renmin University of China, Beijing 100872, People's Republic of China

E-mail: hlei@ruc.edu.cn

Received 10 August 2017, revised 28 September 2017
Accepted for publication 19 October 2017
Published 21 November 2017

Abstract

We study the electric transport properties of $Li_x(NH_3)_yFe_2(Te_zSe_{1-z})_2$ single crystals with $z = 0$ and 0.6 in the mixed state. Thermally-activated flux-flow, vortex glass and flux-flow Hall effect (FFHE) behaviors are observed. Experimental results show that there are rich vortex phases existing in these systems and the vortex liquid states occupy broad regions of phase diagrams. Further analysis suggests that thermal fluctuation plays an important role in the vortex phase diagrams of $Li_x(NH_3)_yFe_2(Te_zSe_{1-z})_2$. Moreover, for $Li_x(NH_3)_yFe_2Se_2$, there is no sign reversal of FFHE in the mixed state and a scaling behavior $|\rho_{xy}(\mu_0 H)| = A\rho_{xx}(\mu_0 H)^{\beta}$ with $\beta \sim 2.0$ is observed.

Keywords: $Li_x(NH_3)_yFe_2(Te_zSe_{1-z})_2$, single crystals, electric transport properties, mixed state, thermally-activated flux-flow, vortex glass, flux-flow Hall effect

(Some figures may appear in colour only in the online journal)

1. Introduction

Since the discovery of LaOFeAs [1], iron-based superconductors (IBSCs) have become another family of high-T_c superconductors besides cuprate SCs and have attracted intense attention. On the one hand, because of high superconducting transition temperature T_c and large upper critical fields $\mu_0 H_{c2}$, IBSCs are important not only for basic science but also for practical applications. On the other hand, the values of Ginzburg number Gi ranging from 10^{-4} to 10^{-2} in IBSCs indicate that the effect of thermal fluctuation varies in different members of IBSCs. It leads to rich vortex phase diagrams in these SCs [2].

Among IBSCs, the iron-chalcogenide SC FeSe has a relative low and nearly isotropic $\mu_0 H_{c2}$ with low T_c (~8 K) [3, 4] when compared to iron-pnictide SCs [5]. After intercalating alkali metals A in between FeSe layers using a high-temperature synthesis method, the T_c can be dramatically enhanced up to about 31 K for $A_xFe_{2-y}Se_2$ [6]. However, the obvious mesoscopic phase separation between the superconducting phase and the inter-grown antiferromagnetic insulating phase in these compounds makes it difficult to study their intrinsic physical properties [7]. On the other hand, superconducting $(Li_{1-x}Fe_x)$OHFeSe synthesized by a novel hydrothermal method exhibits the features of high T_c (>40 K), rather large $\mu_0 H_{c2}$ (>60 T for $H||c$) and Gi ($\sim 1.3 \times 10^{-2}$) [8–11]. It results in the existence of various vortex phases in $(Li_{1-x}Fe_x)$OHFeSe single crystals [11, 12].

Besides $A_xFe_{2-y}Se_2$ and $(Li_{1-x}Fe_x)$OHFeSe, AM-NH_3 cointercalated FeSe (AM = alkali, alkali-earth, and rare-earth metals) forms another class of iron-chalcogenide SCs with high T_c (>40 K) [13–17]. But the absence of single crystals impedes the study of the transport properties and vortex dynamics of these SCs. Very recently, we have grown $Li_x(NH_3)_yFe_2Se_2$ single crystals successfully and they show rather high T_c and $\mu_0 H_{c2}$ with significant anisotropy [18], similar to $(Li_{1-x}Fe_x)$OHFeSe. In this work, we present a comprehensive study of the electric transport properties of $Li_x(NH_3)_yFe_2(Te_zSe_{1-z})_2$ single crystals with $z = 0$ and 0.6 (denoted as LiFeSe-122 and LiFeTeSe-122 for brevity) in the mixed state. The observed thermally-activated flux-flow (TAFF), vortex glass (VG) and flux-flow Hall effect (FFHE) behaviors indicate that there are diverse vortex phases and rather broad vortex liquid region in these systems. Large Gi in

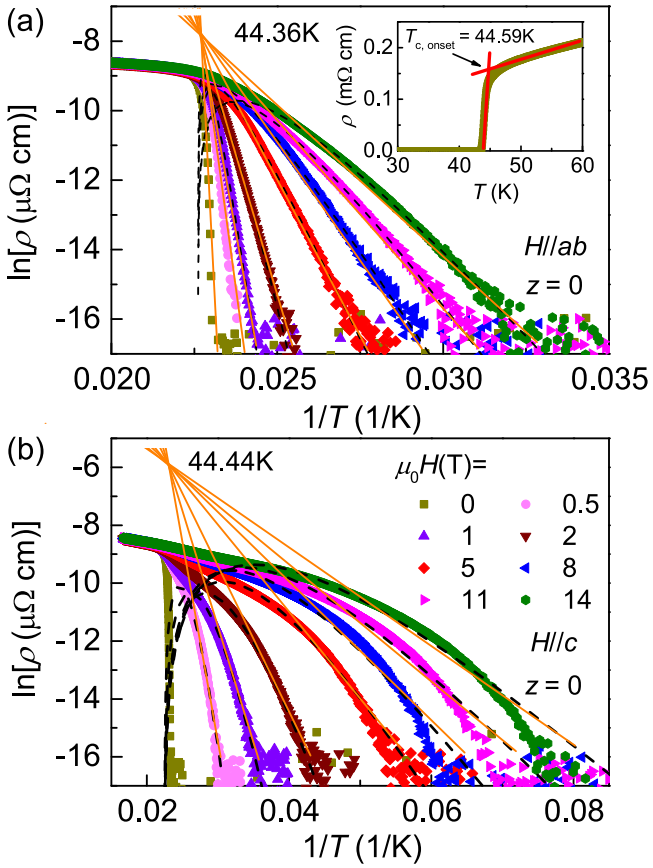

Figure 1. (a) and (b) The natural logarithm of $\rho(T, \mu_0 H)$ of LiFeSe-122 as a function of inverse of temperature at various fields for $H||ab$ and $H||c$, respectively. The orange solid and black dashed lines are fitting results from the Arrhenius relation and equation (5). Inset: temperature dependence of in-plane resistivity $\rho(T)$ for LiFeSe-122 at zero field.

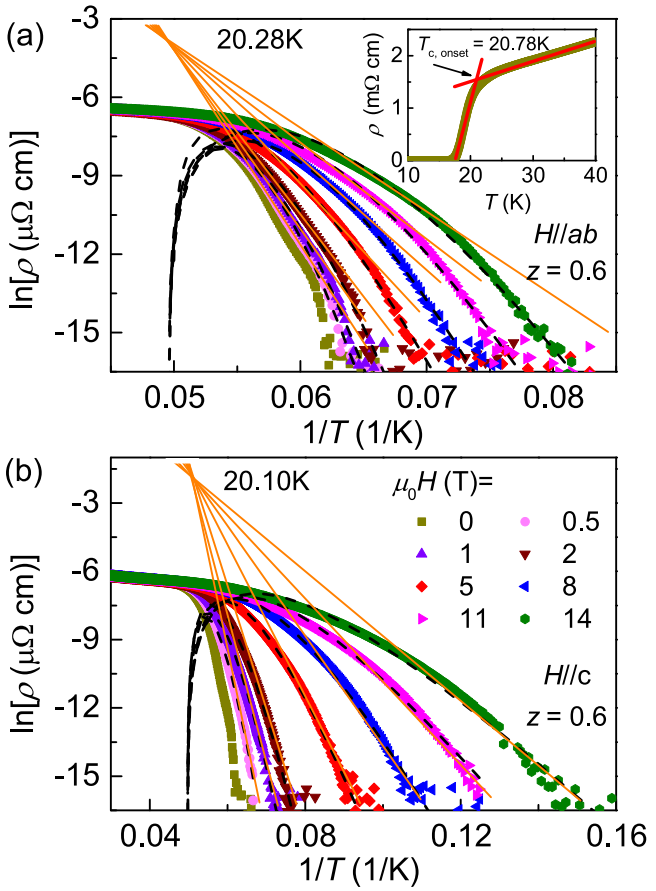

Figure 2. (a) and (b) ln $\rho(T, \mu_0 H)$ versus $1/T$ for LiFeTeSe-122 at various fields with $H||ab$ and $H||c$, respectively. The orange solid and black dashed lines are the fitting results from the Arrhenius relation and equation (5). Inset : temperature dependence of in-plane resistivity $\rho(T)$ for LiFeTeSe-122 at zero field.

LiFeSe-122 suggests the thermal fluctuation is essential to vortex dynamics. Moreover, the scaling behavior of $|\rho_{xy}(\mu_0 H)| = A\rho_{xx}(\mu_0 H)^{\beta}$ with $\beta \sim 2$ implies that the strength of the pinning force is relatively weak in LiFeSe-122 when $H||c$ and the temperature is close to T_c. On the other hand, with Te doping, the *Gi* decreases with decreased T_c.

2. Experiment

Single crystals of LiFeSe-122 and LiFeTeSe-122 were synthesized via the low-temperature ammonothermal technique. The detailed experimental procedure and characterizations of crystals were described in previous works [18, 19]. The elemental analysis was performed using the inductively coupled plasma atomic emission spectroscopy (ICP-AES) and the atomic ratio of $Li_x(NH_3)_yFe_2(Te_zSe_{1-z})_2$ single crystals used in this study is Li : Fe : Se = 0.18 : 1 : 0.9 for $z = 0$ and Li : Fe : Te : Se = 0.16 : 1 : 0.60 : 0.38 for $z = 0.6$, respectively. Electrical transport measurements were performed using a four-probe configuration with current flowing in the *ab* plane of crystals in a Quantum Design PPMS-14. The Hall resistivity was obtained from the difference of the transverse resistivity measured at the positive and negative fields in order to remove the longitudinal resistivity contribution due to voltage probe misalignment, i.e. $\rho_{xy}(\mu_0 H) = [\rho(+\mu_0 H) - \rho(-\mu_0 H)]/2$.

3. Results and discussions

Figures 1 and 2 present the longitudinal resistivity $\rho(T, \mu_0 H)$ of LiFeSe-122 and LiFeTeSe-122 single crystals near the superconducting transition region for $H||ab$ and $H||c$, respectively. The field-induced broadenings of resistive transitions and resistive tail behaviors are obvious, especially for the field along the *c* axis. Similar behaviors have also been observed in (Li, Fe)OHFeSe, $SmFeAsO_{0.85}$ and cuprates [9, 12, 20, 21]. It can be ascribed to field-induced TAFF. Based on theoretical model describing the TAFF behavior, the resistivity in the TAFF region can be expressed as [22–24]:

$$\rho = (2\nu_0 LB/J)\exp(-J_{c0}BVL/T)\sinh(JBVL/T) \qquad (1)$$

where ν_0 is an attempt frequency for a flux bundle hopping, L is the hopping distance, B is the magnetic induction, J is the

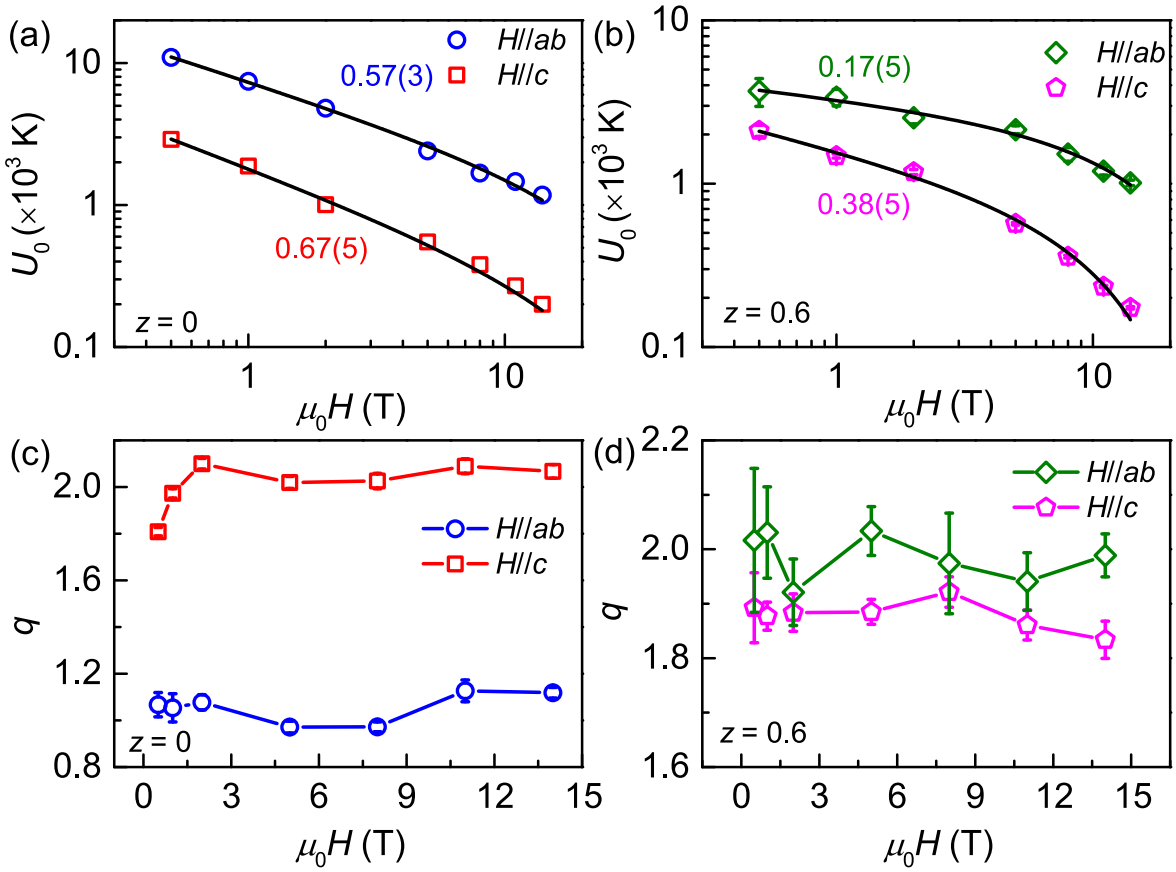

Figure 3. Field dependence of (a, b) U_0 and (c, d) q obtained from the fits of the resistivity in the TAFF region using equation (5) for LiFeSe-122 and LiFeTeSe-122, respectively. The solid lines in (a) and (b) are fits using equation (6) and the values beside the lines are fitted γ.

applied current density, J_{c0} is the critical current density in the absence of flux creep, V is the bundle volume and T is the temperature. If J is small enough and $JBVL/T \ll 1$, equation (1) can be expressed as

$$\rho = (2\rho_c U/T)\exp(-U/T) = \rho_{0f}\exp(-U/T) \quad (2)$$

where $U = J_{c0}BVL$ is the thermally-activated energy (TAE) or flux-pinning energy, and $\rho_c = \nu_0 LB/J_{c0}$, which is usually considered to be temperature independent. According to the condensation model, $U(T, \mu_0 H) = U_0(\mu_0 H)(1-t)^q$, where $t = T/T_c$ (T_c is the superconducting transition temperature), $q = 2 - n/2$ (n depends on the dimensionality of the vortex system with the range from 0 to 3) and $U_0(\mu_0 H)$ is the apparent activated energy [22, 24, 25]. Generally assuming $n = 2$ and the prefactor ρ_{0f} is a constant as for cuprate SCs [22], we can obtain

$$\ln\rho(T, \mu_0 H) = \ln\rho_0(\mu_0 H) - U_0(\mu_0 H)/T \quad (3)$$

and

$$\ln\rho_0(\mu_0 H) = \ln\rho_{0f} + U_0(\mu_0 H)/T_c. \quad (4)$$

Thus, there is a linear relationship between $\ln\rho(T, \mu_0 H)$ and $1/T$ in TAFF region (Arrhenius relation) and the slope and y-axial intercept correspond to $U_0(\mu_0 H)$ and $\ln\rho_0(\mu_0 H)$, respectively. As shown in figures 1(a) and (b), the solid lines represent the results of linear fitting in the TAFF region using the Arrhenius relation. All the linear fittings cross at T_{cross} approximately, which are about 44.36 K and 44.44 K for $H\|ab$ and $H\|c$, respectively. Ideally, all the lines at different fields should be crossed into one point, T_{cross}, which should be equal to T_c [26]. Obviously, the values of T_{cross} are consistent with the $T_{c,onset}$ in the $\rho(T)$ curves for both field directions (44.59 K and 44.56 K).

Although the $\ln\rho(T, \mu_0 H)$ versus $1/T$ can be fitted linearly, there are relative large fitting errors for $H\|c$ because the Arrhenius relation can only be satisfied in a narrow region. It suggests that the assumptions of linear temperature dependence of $U(T, \mu_0 H)$ and temperature-independent ρ_{0f} may not be valid, leading to $\ln\rho(T, \mu_0 H)$ versus $1/T$ deviating from the Arrhenius relation [27]. Using the relation $U(T, \mu_0 H) = U_0(\mu_0 H)(1-t)^q$, the equation (2) can be rewritten as

$$\ln\rho = \ln(2\rho_c U_0) + q\ln(1-t) - \ln T - U_0(1-t)^q/T \quad (5)$$

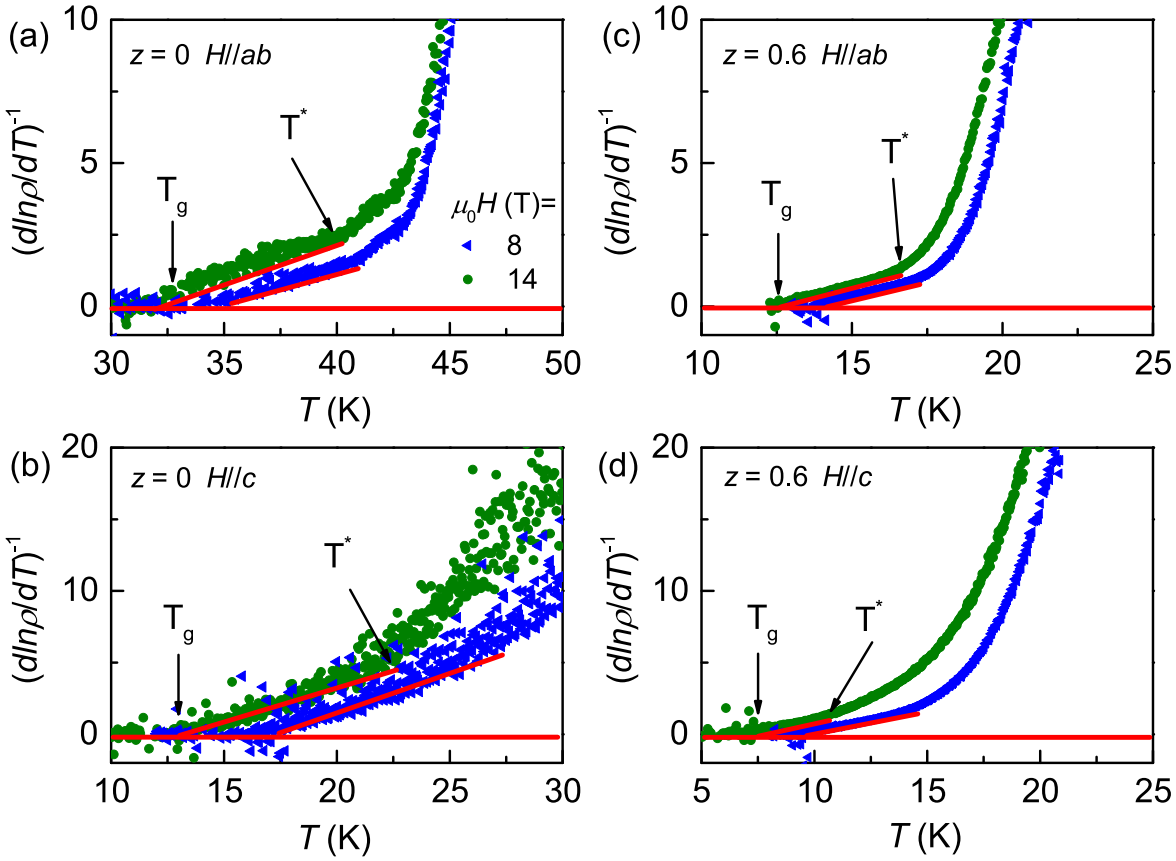

Figure 4. $(d\ln\rho/dT)^{-1}$ versus T at $\mu_0 H = 8$ and 14 T of (a, b) LiFeSe-122 and (c, d) LiFeTeSe-122 for $H||ab$ and $H||c$, respectively.

where ρ_c and U_0 are temperature independent and the value of T_c is derived from the Arrhenius relation. All fits (black dashed lines) using equation (5) are also plotted in figures 1(a) and (b). It can be seen that this more general method is in better agreement with experimental data than the Arrhenius relation, especially for $H||c$.

The same analysis procedure can be applied to LiFeTeSe-122. As shown in figures 2(a) and (b), T_{cross} obtained from the linear fitting is about 20.28 K and 20.10 K for $H||ab$ and $H||c$, respectively. The values of T_{cross} are close to the $T_{c,onset}$ in the $\rho(T)$ curves (20.78 K and 20.79 K). In contrast to LiFeSe-122, the $\ln\rho(T, \mu_0 H)$ of LiFeTeSe-122 for both field directions are not linearly proportional to $1/T$, i.e. the Arrhenius relation cannot capture the bending trends of curves. However, the data can be fitted well using equation (5).

The fitted U_0 and q at various fields for both samples are shown in figure 3. According to the Anderson-Kim model, $U_0(\mu_0 H)$ is related to the effective pinning energy. $U_0(\mu_0 H)$ for $H||ab$ are much larger than that for $H||c$ in both crystals (figures 3(a) and (b)), confirming that the flux pinning is much stronger for $H||ab$. It is consistent with the layered structure of $Li_x(NH_3)_yFe_2(Te_zSe_{1-z})_2$. When compared with $U_0(\mu_0 H) \sim 250$ K at $\mu_0 H = 0.5$ T for FeSe [28], the $U_0(\mu_0 H)$ for $H||c$ at the same field enhances to about 10^4 K in LiFeSe-122, indicating a much stronger vortex-pinning energy with an increased T_c after intercalating the Li-NH_3 layers in between FeSe layers. In contrast, the value of $U_0(\mu_0 H)$ remains in the same order of magnitude ($10^2 \sim 10^3$ K) after intercalating the Li-NH_3 layers into $FeTe_{1-x}Se_x$ [29, 30]. That is to say, their effective pinning energies are comparable. According to Kramer's law [31], the field dependence of $U_0(\mu_0 H)$ can be expressed as

$$U_0(\mu_0 H) = a(\mu_0 H)^{\gamma}(1 - \mu_0 H/\mu_0 H_{irr})^{\delta} \quad (6)$$

where $\mu_0 H_{irr}$ is an irreversible field and γ, δ are scaling parameters. In LiFeSe-122, when assuming $\delta = 2$, the field is parallel to ab plane, the value of γ is 0.57(3) and 0.67(5) for $H||ab$ and $H||c$, respectively (figure 3(a)). On the other hand, the value of γ is 0.17(5) for $H||ab$ and 0.38(5) for $H||c$ in LiFeTeSe-122 (figure 3(b)). The weak field dependence of U_0 implies that single-vortex pinning should be dominant in LiFeTeSe-122. In contrast, the faster decreases of $U_0(\mu_0 H)$ in LiFeSe-122 imply that the collective flux pinning may dominate [32]. The better fits using equation (5) than the Arrhenius relation can be partially ascribed to considering the temperature dependence of prefactor ρ_{0f}. When the assumption of $U \gg T$ with $q = 1$ is satisfied, the Arrhenius relation is valid and it can well describe the TAFF behavior, as in LiFeSe-122 for $H||ab$. But because the obtained U_0 of LiFeSe-122 for $H||c$ and LiFeTeSe-122 for both field directions are much smaller than that of LiFeSe-122 for $H||ab$, the assumption of temperature-independent ρ_{0f}, i.e. $U \gg T$, might be improper and the Arrhenius relation will become invalid.

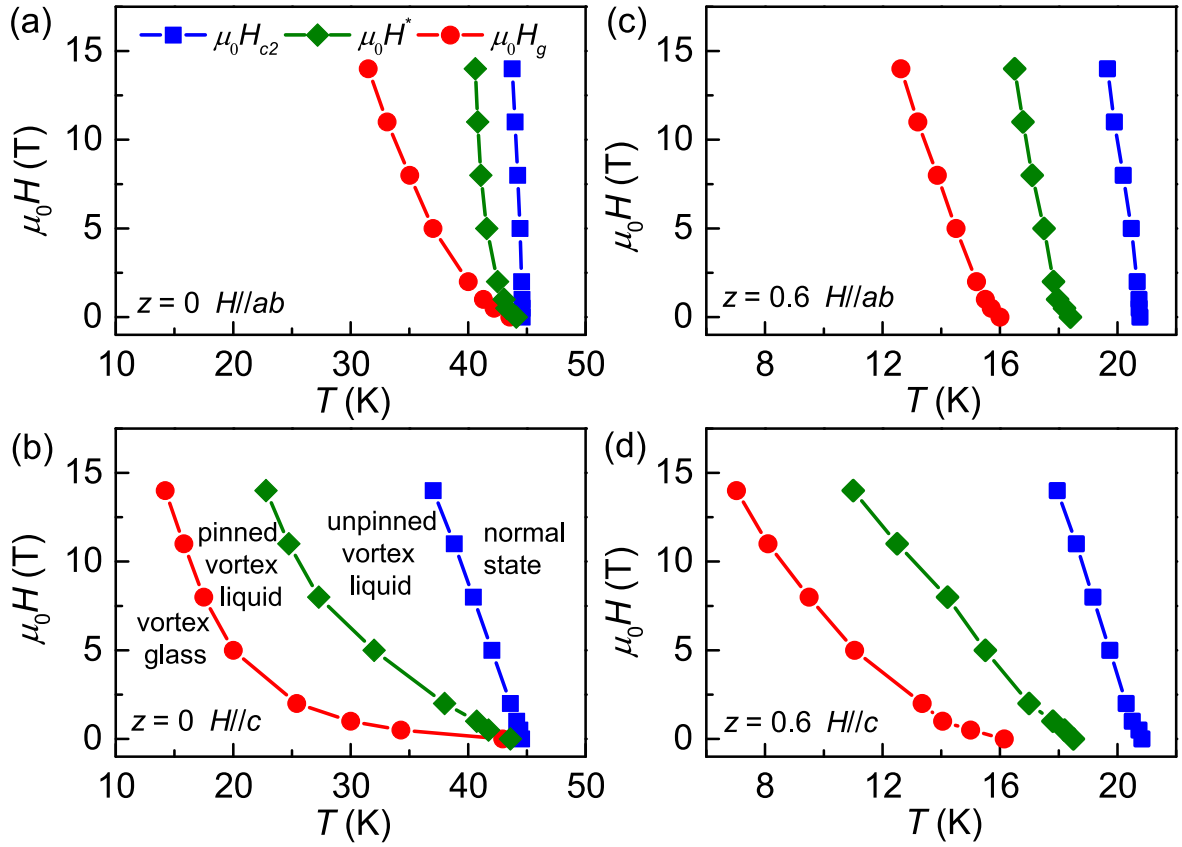

Figure 5. The vortex phase diagrams ($\mu_0H - T$) of (a, b) LiFeSe-122 and (c, d) LiFeTeSe-122 for $H||ab$ and $H||c$, respectively. μ_0H_{c2} is the upper critical field defined from the 90% ρ_n; μ_0H^* represents the transition from the unpinned to the strongly pinned vortex region and μ_0H_g represents the transition from vortex liquid to glass region.

As shown in figures 3(c) and (d), the q for both crystals are almost independent of the field strength for both directions. When $H||c$, the values of q for both samples are about 2, but it changes from 1 in LiFeSe-122 to 2 in LiFeTeSe-122 when $H||ab$. The $q = 1$ for $H||ab$ in LiFeSe-122 is consistent with the good linear behavior of ln $\rho(T, \mu_0H)$ versus $1/T$ shown in figure 1(a). In contrast, the value of $q = 2$ should be another reason leading to the deviation of experimental curves from the Arrhenius relation.

According to the VG model [33, 34], the linear resistivity disappears as a power law

$$\rho = \rho_0|\frac{T}{T_g} - 1|^s \tag{7}$$

close to the glass transition temperature, T_g. In equation (7), ρ_0 is identified as a characteristic resistivity and should in some way be related to the normal state resistivity and s is the glass critical exponent. T_g can be extracted by applying the relation $(d \ln \rho/dT)^{-1} \propto (T - T_g)$ to the resistive tail, and T^* is defined as the temperature deviating from the straight line, as shown in figure 4.

Based on the values of T_g and T^* extracted from VG model and μ_0H_{c2} defined from the 90% ρ_n, we plot the vortex phase diagrams of LiFeSe-122 and LiFeTeSe-122 (figure 5). The different regions indicate different flux-pinning mechanisms. The region below the μ_0H_g line is a vortex glass phase and the region above μ_0H_{c2} is the normal state, while the region between μ_0H_g and μ_0H_{c2} is the vortex liquid phase. Besides, μ_0H^* represents the divider of unpinned and strongly pinned regions of vortex liquid. Obviously, the vortex liquid region is broad in these crystals, especially in LiFeSe-122 with $H||c$, suggesting a weak vortex-pinning ability even at relative low field in this system when T approaches T_c.

Because the resistive transition curve $\rho(T, \mu_0H)$ not only shifts but also broadens when the field increases, it suggests that thermal fluctuation is essential to vortex dynamics in these materials. The strength of thermal fluctuations can be quantified by $Gi = (\gamma^2/2)[(\mu_0k_BT_c)/(4\pi B_c^2(0)\xi_{ab}^3(0))]^2$ [35], where γ is the electronic mass anisotropy, $B_c(0) = \Phi_0/(2\sqrt{2}\pi\lambda_{ab}(0)\xi_{ab}(0))$ is the thermodynamic critical field, Φ_0 is the flux quantum, $\xi_{ab}(0)$ and $\lambda_{ab}(0)$ is the coherence length and penetration depth at 0 K for $H||ab$. With $\gamma = \xi_{ab}/\xi_c$, we obtain $Gi = [(2\pi\mu_0K_BT_c\lambda_{ab}^2(0))/(\Phi_0^2\xi_c(0))]^2/2$, where $\xi_c(0)$ is the coherence length at 0 K for $H||c$. Assuming $\lambda_{ab}(0) = 200$ nm is the same as (Li, Fe)OHFeSe [11], the value of Gi is 1.4×10^{-2} and 2.8×10^{-4} for LiFeSe-122 and LiFeTeSe-122 with $\xi_c(0) = 0.27$ and 0.9 nm derived from $\mu_0H_{c2}(0)$. The value of Gi for LiFeSe-122 is comparable with (Li, Fe)OHFeSe (1.3×10^{-2}) and YBCO (10^{-2}), but much larger than that of LiFeTeSe-122 [11, 35]. It is consistent with the more obvious broadening of $\rho(T, \mu_0H)$

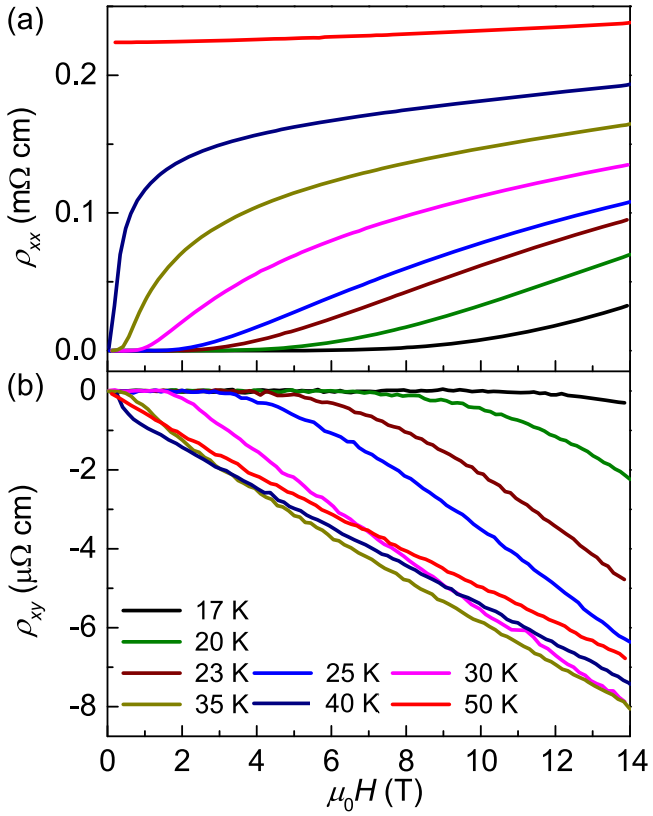

Figure 6. Field dependence of (a) longitudinal resistivity $\rho_{xx}(\mu_0 H)$ and (b) Hall resistivity $\rho_{xy}(\mu_0 H)$ of LiFeSe-122 at various temperatures for $H||c$.

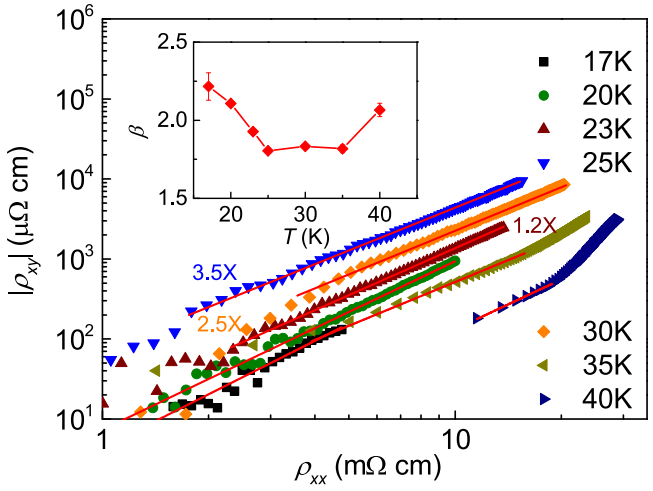

Figure 7. $|\rho_{xy}|$ versus ρ at various temperatures for LiFeSe-122. The solid lines are fitting results using the scaling behavior $|\rho_{xy}(\mu_0 H)| = A\rho_{xx}(\mu_0 H)^{\beta}$. Inset: temperature dependence of $\beta(T)$.

in LiFeSe-122, especially for $H||c$. The remarkable thermally-activated vortex dynamics in LiFeSe-122 also lead to the wider region of vortex glass/liquid states in vortex phase diagrams when compared to LiFeTeSe-122.

The Hall effect in the mixed state is another measurement to study vortex dynamics. Figure 6(a) shows the field dependence of longitudinal resistivity $\rho_{xx}(\mu_0 H)$ of LiFeSe-122 in the temperature range of 17 K–50 K when $H||c$. With increasing field, superconductivity is suppressed gradually and the transition of $\rho(\mu_0 H)$ shifts to lower magnetic fields when temperature increases. $\rho_{xx}(\mu_0 H)$ shows a weak positive magnetoresistance at the normal state ($T = 50$ K), consistent with previous results [18]. As shown in figure 6(b), at the mixed state, the Hall resistivity $\rho_{xy}(\mu_0 H)$ at low field is zero and becomes negative with increased absolute values at the high fields. The high-field values of $\rho_{xy}(\mu_0 H)$ gradually reach that in the normal state when temperature is slightly higher than T_c. The sign of the Hall resistivity is negative, indicating that the electron type carriers dominate in the mixed state as well as in the normal state, consistent with the electron doping in LiFeSe-122. Moreover, there is no sign reversal of $\rho_{xy}(\mu_0 H)$ in the mixed state, which is often observed in cuprates [36, 37].

Furthermore, there is a scaling behavior of $|\rho_{xy}(\mu_0 H)| = A\rho_{xx}(\mu_0 H)^{\beta}$ in LiFeSe-122 (figure 7) and the fitted values of β are close to 2 in the whole measuring temperature range. Different values of β have been observed in IBSCs and cuprate SCs, such as Fe(Te, S) ($\beta = 0.9$–1.0) [26], $Ba(Fe_{0.9}Co_{0.1})As_2$ ($\beta = 2.0(2)$) [38], and $Bi_2Sr_2CaCu_2O_y$ ($\beta = 2.0 \pm 0.1$) [39]. A number of theories have been proposed to explain the value of β. For example, when considering the effect of pinning on the Hall resistivity, Vinokur *et al* proposed a phenomenological model where $\beta = 2.0$ in the TAFF region [40]. Additionally, a unified theory for the Hall effect including both the pinning effect and thermal fluctuations was developed by Wang, Dong, and Ting [41, 42]. They explained scaling behavior by taking into account the backflow current effect on flux motion due to pinning and pointed out β changing from 2 to 1.5 for increasing pinning force. The exponent $\beta \sim 2.0$ and the absence of sign change of $\rho_{xy}(\mu_0 H)$ for LiFeSe-122 single crystals imply that the strength of pinning force is relatively weak when $H||c$ and $T \to T_c$, consistent with the low TAE in the same field direction shown above.

4. Conclusion

In summary, field-induced resistive broadenings of superconducting transitions and resistive tail behaviors have been observed in $Li_x(NH_3)_yFe_2(Te_zSe_{1-z})_2$ single crystals. Detailed analysis shows that these results are associated with TAFF and VG behaviors. Moreover, thermal fluctuation plays an important role in the vortex dynamics of $Li_x(NH_3)_yFe_2(Te_zSe_{1-z})_2$ single crystals, especially for LiFeSe-122, resulting in broad vortex liquid regions in the vortex phase diagrams. The FFHE with $\beta \sim 2$ indicates the relatively weak vortex-pinning force in LiFeSe-122 when the magnetic field is along the c axis and T approaches T_c.

Acknowledgments

This work was supported by the Ministry of Science and Technology of China (2016YFA0300504), the National Natural Science Foundation of China (No. 11574394 and

no. 11774423), the Fundamental Research Funds for the Central Universities, and the Research Funds of Renmin University of China (RUC) (15XNLF06, 15XNLQ07).

ORCID iDs

Shanshan Sun https://orcid.org/0000-0002-8686-0524
Hechang Lei https://orcid.org/0000-0003-0850-8514

References

[1] Kamihara Y, Watanabe T, Hirano M and Hosono H 2008 *J. Am. Chem. Soc.* **130** 3296
[2] Gurevich A 2011 *Rep. Prog. Phys.* **74** 124501
[3] Hsu F C *et al* 2008 *Proc. Natl. Acad. Sci. USA* **105** 14262
[4] Vedeneev S I, Piot B A, Maude D K and Sadakov A V 2013 *Phys. Rev.* B **87** 134512
[5] Hunte F, Jaroszynski J, Gurevich A, Larbalestier D C, Jin R, Sefat A S, McGuire M A, Sales B C, Christen D K and Mandrus D 2008 *Nature* **453** 903
[6] Guo J G, Jin S F, Wang G, Wang S C, Zhu K X, Zhou T T, He M and Chen X L 2010 *Phys. Rev.* B **82** 180520(R)
[7] Chen F *et al* 2011 *Phys. Rev.* X **1** 021020
[8] Lu X F *et al* 2015 *Nat. Mater.* **14** 325
[9] Dong X *et al* 2015 *Phys. Rev.* B **92** 064515
[10] Wang Z, Yuan J, Wosnitza J, Zhou H, Huang Y, Jin K, Zhou F, Dong X and Zhao Z 2017 *J. Phys.: Condens. Matter* **29** 025701
[11] Yi X, Wang C, Tang Q, Peng T, Qiu Y, Xu J, Sun H, Luo Y and Yu B 2016 *Supercond. Sci. Technol.* **29** 105015
[12] Lin H, Xing J, Zhu X Y, Yang H and Wen H H 2016 *Sci. Chi. PMA.* **59** 657404
[13] Ying T P, Chen X L, Wang G, Jin S F, Zhou T T, Lai X F, Zhang H and Wang W Y 2012 *Sci. Rep.* **2** 426
[14] Scheidt E-W, Hathwar V R, Schmitz D, Dunbar A, Scherer W, Mayr F, Tsurkan V, Deisenhofer J and Loidl A 2012 *Eur. Phys. J.* B **85** 279
[15] Ying T P, Chen X L, Wang G, Jin S F, Lai X F, Zhou T T, Zhang H, Shen S J and Wang W Y 2013 *J. Am. Chem. Soc.* **135** 2951
[16] Burrard-Lucas M *et al* 2013 *Nat. Mater.* **12** 15
[17] Sedlmaier S J, Cassidy S J, Morris R G, Drakopoulos M, Reinhard C, Moorhouse S J, O'Hare D, Manuel P, Khalyyavin D and Clarke S J 2014 *J. Am. Chem. Soc.* **136** 630
[18] Sun S S, Wang S H, Yu R and Lei H C 2017 *Phys. Rev.* B **96** 064512
[19] Wang S H, Sun S S and Lei H C 2017 *Supercond. Sci. Technol.* **30** 115005
[20] Lee H-S, Bartkowiak M, Park J-H, Lee J-Y, Kim J-Y, Sung N-H, Cho B K, Jung C-U, Kim J S and Lee H-J 2009 *Phys. Rev.* B **80** 144512
[21] Fendrich J A, Kwok W K, Giapintzakis J, van der Beck C J, Vinokur V M, Fleshier S, Welp U, Viswanathan H K and Crabtree G W 1995 *Phys. Rev. Lett.* **74** 1210
[22] Palstra T T M, Batlogg B, Schneemeyer L F and Waszczak J V 1988 *Phys. Rev. Lett.* **61** 1662
[23] Blatter G, Feigel'man M V, Geshkenbein V B, Larkin A I and Vinokur V M 1994 *Rev. Mod. Phys.* **66** 1125
[24] Palstra T T M, Batlogg B, van Dover R B, Schneemeyer I F and Waszczak J V 1990 *Phys. Rev.* B **41** 6621
[25] Brandt E H 1995 *Rep. Prog. Phys.* **58** 1465
[26] Lei H C, Hu R W, Choi E S and Petrovic C 2010 *Phys. Rev.* B **82** 134525
[27] Zhang Y Z, Wen H H and Wang Z 2006 *Phys. Rev.* B **74** 144521
[28] Lei H C, Hu R W and Petrovic C 2011 *Phys. Rev.* B **84** 014520
[29] Shahbazi M, Wang X L, Ghorbani S R, Dou S X and Lin C T 2015 *Physica* C **519** 60
[30] Wu Z F, Tao J, Xu X B, Qiu L, Yang S G and Wang Z H 2016 *Physica* C **528** 39
[31] Thompson J R, Sorge K D, Cantoni C, Kerchner H R, Christen D K and Paranthaman M 2005 *Supercond. Sci. Technol.* **18** 970–6
[32] Yeshurun Y and Malozemoff A P 1988 *Phys. Rev. Lett.* **60** 2202
[33] Espinosa-Arronte B and Andersson M 2005 *Phys. Rev.* B **71** 024507
[34] Andersson M, Rydh A and Rapp Ö 2001 *Phys. Rev.* B **63** 184511
[35] Eley S, Miura M, Maiorov B and Civale L 2017 *Nat. Mater.* **16** 409
[36] Cagigal M, Fontcuberta J, Crusellas M A, Vicent J L and Piñol S 1995 *Physica* C **248** 155
[37] Hagen S J *et al* 1993 *Phys. Rev.* B **47** 1064
[38] Wang L M, Sou U-C, Yang H C, Chang L J, Cheng C-M, Tsuei K-D, Su Y, Wolf T and Adelmann P 2011 *Phys. Rev.* B **83** 134506
[39] Samoilov A V 1993 *Phys. Rev. Lett.* **71** 617
[40] Vinokur V M, Geshkenbein V B, Feigel'man M V and Blatter G 1993 *Phys. Rev. Lett.* **71** 1242
[41] Wang Z D and Ting C S 1991 *Phys. Rev. Lett.* **67** 3618
[42] Wang Z D, Dong J and Ting C S 1994 *Phys. Rev. Lett.* **72** 3875